Hyperspectral Infrared Sounder Cloud Detection Using Deep Neural Network Model

Qian Liu, Hui Xu, Dexuan Sha, Tsengdar Lee, Daniel Q. Duffy, Jeff Walter, and Chaowei Yang, *Member, IEEE*

***Abstract*— Detection of cloud contaminated field of views (FOV) from satellite hyperspectral infrared sounders is essential for numerical weather prediction. A new cloud detection model is developed for the cross-track infrared sounder (CrIS) using the artificial deep neural network (DNN) technique. The truth cloud information used is from another instrument of Visible Infrared Imaging Radiometer Suite (VIIRS) deployed on the same platform of CrIS. The training data set is built from CrIS–VIIRS collocated measurements randomly selected from different months to represent different atmospheric and surface conditions. Then, we use the VIIRS cloud mask collocated within the CrIS footprint to train the CrIS spectra for cloud detection. Specifically, the CrIS spectra were transformed into their principal components (PCs), with only the top 75 PCs used as the predictors rather than the entire CrIS channels, for the purpose of better regression and convergence during the training process and faster prediction. Results were examined globally by the considered truth derived from the VIIRS cloud mask. Generally, the spatial distribution of the proposed CrIS cloud detection result agrees with that from the VIIRS, with a high model accuracy of 93%. Further analysis indicates that the proposed CrIS cloud detection result is slightly better over daytime than nighttime with the accuracy values of 94% versus 91%. The ocean areas have a higher cloud detection accuracy than continental land with accuracy values of 95% versus 88%. In addition, sometimes the DNN model would recognize the thin cloud as clear sky, as their spectra are very similar to each other. False detected pixels are also found over snow- or ice-covered and desert areas. This is possibly due to the VIIRS cloud mask that has a relatively low accuracy over these areas.**

***Index Terms*— Cloud detection, cross-track infrared sounder (CrIS), deep neural network (DNN), Geo artificial intelligence (GeoAI), hyperspectral infrared sounder.**

Manuscript received April 3, 2020; revised June 8, 2020 and July 14, 2020; accepted August 27, 2020. This work was supported in part by the National Aeronautics and Space Administration (NASA) under Grant 80NSSC19 P2033 and in part by the National Science Foundation (NSF) under Grant CNS 1841520 and Grant ACI 1835507. *(Corresponding author: Chaowei Yang.)*

Qian Liu, Dexuan Sha, and Chaowei Yang are with the Department of Geography and Geoinformation Science, George Mason University, Fairfax, VA 22030 USA (e-mail: qliu6@gmu.edu; dsha@gmu.edu; cyang3@gmu.edu).

Hui Xu is with the Earth System Science Interdisciplinary Research Center, University of Maryland, College Park, MD 20740 USA (e-mail: huixu@umd.edu).

Tsengdar Lee is with the NASA Headquarters, Washington DC 20546 USA (e-mail: tsengdar.j.lee@nasa.gov).

Daniel Q. Duffy is with the NASA Center for Climate Simulation, Greenbelt, MD 20771 USA (e-mail: daniel.q.duffy@nasa.gov).

Jeff Walter is with the NASA Langley Research Center, Atmospheric Science Data Center (ASDC), Hampton, VA 23666 USA (e-mail: jeff.walter@nasa.gov).

Color versions of one or more of the figures in this letter are available online at http://ieeexplore.ieee.org.

Digital Object Identifier 10.1109/LGRS.2020.3023683

I. Introduction

THE cross-track infrared sounder (CrIS), a hyperspectral infrared sounder flying on the afternoon orbit Suomi National Polar-orbiting Partnership (SNPP) and National Oceanic and Atmospheric Administration (NOAA)-20 satellites, provides improved atmospheric temperature and moisture sounding information for weather and climate applications [1]. It measures the earth in three discrete spectral regions: long-wave (LW) band at 650–1095 cm^{-1}, middle-wave (MW) band at 1210–1750 cm^{-1}, and short-wave (SW) band at 2155–2550 cm^{-1}. By design, CrIS has a large circular footprint of 14 km at nadir, resulting in its field of view (FOV) often containing clouds, especially over the atmospheric window channels. Clouds influence the infrared radiance due to their strong absorption and scattering in the infrared spectral region. They can block hyperspectral infrared sounders from correctly sensing atmospheric profiles and underlying surfaces. Unlike microwave data, numerical weather prediction (NWP) models only assimilate clear-sky measurements from hyperspectral infrared sounders, as it is hard to precisely simulate the cloud contaminated radiances with the forward radiative model [2]. Any infrared sounding data should be filtered by a proper cloud detection algorithm before being assimilated into the NWP models. Therefore, it is essential to develop an effective cloud clearing algorithm for the operational NWP models as well as other applications in which clear sky is needed.

Many cloud detection methods have been developed for infrared sounders. The channel-dependent cloud detection algorithm [3] has been widely used in the NWP models. The clouds in each channel are determined by the spectral difference between the satellite observations and the cloud-free model forward simulations. To mitigate the disadvantage of model simulation, a double CO_2 band cloud detection method is further developed [4] for CrIS. However, partially cloud detection is challenging for these methods due to the large footprint of sounders. Another way to accurately identify cloud is to use information from multiple instrument pairs. For example, the Atmospheric Infrared Sounder (AIRS) and Advanced Microwave Sounding Unit-A (AMSU-A) cloud clearing method developed by the AIRS Science Team [5]. It is further extended to Infrared Atmospheric Sounding Interferometer (IASI) and AMSU-A, as well as CrIS and Advanced Technology Microwave Sounder (ATMS) within the operational NOAA Unique Combined Atmospheric Processing System (NUCAPS) [6]. These methods get cloud information spatially and reserve the spectral information of infrared sounders for profile retrievals. In addition, infrared sounder clear-sky FOVs can also be determined by a collocated high-spatial-resolution imager, such as the AIRS observations

that are checked individually by their collocated Moderate Resolution Imaging Spectroradiometer (MODIS) cloud mask product [7]. Similar methods were also applied to IASI and the CrIS [8], [9] by using the cloud information measured from their collocated imagers of Advanced Very High-Resolution Radiometer (AVHRR) and Visible Infrared Imaging Radiometer Suite (VIIRS) observations, respectively. As the cloud information is directly derived from the high-spatial-resolution imagers, the subpixel cloud detection for the infrared sounders becomes available with these methods. However, it usually takes time and much effort to do the collocation preprocessing and thus increases the complexity of the operational cloud detection algorithm.

With the advancements in artificial intelligence (AI) [10], machine and deep learning models have been developed to investigate spatiotemporal climatological phenomena in recent years [11], [12]. Deep neural network (DNN) is one of the many AI models with multiple hidden layers among the input and output layers. It provides better solutions for complicated problems (e.g., high-dimensional issues with nonlinearity) that usually have no direct mathematical answers and could benefit from an effective feature extraction approach for hyperspectral data [13]. The DNN model is widely used for satellite imagery classifications, atmospheric and surface parameter retrievals, and NWP [14]. This letter initially explores the ability of DNN to detect cloudy FOVs of the hyperspectral infrared sounders by using CrIS as an example, providing insight into infrared sounder target detection. Particularly and during the model training process, cloud mask from the VIIRS is used in determining the CrIS cloud contaminated FOVs. The VIIRS is a high-spatial-resolution imager deployed on the same satellite platforms of CrIS. Unlike the previous methods (all sounder FOVs are checked by their collocated imager cloud product one-by-one), the proposed cloud detection model directly uses the imager's cloud information to train the sounder spectra with DNN for cloud detection, which avoids the time-consuming steps of collocation preprocessing and makes it easier to implement in operational systems and adopt by researchers.

This letter is organized as follows. Section II describes the data set and methodology. Section III presents the case analysis and accuracy validation, and finally, Section IV draws conclusions.

II. Data and Methods

A. Data Product

The CrIS is a Michelson interferometer onboard the SNPP and NOAA-20 spacecrafts in a Sun-synchronous orbit. It measures the spectrum in three infrared bands concurrently by a 3×3 detector array, as described in Section I. The combined nine detectors define the field of regard (FOR). CrIS collects 34 FORs in each scan, including 30 earth, 2 deep space, and 2 internal calibration target measurements. It provides a total of 2211 radiance channels in the full spectral resolution (FSR) mode with an equal interval of 0.625 cm^{-1} [1].

The VIIRS is a whiskbroom scanning radiometer onboard the same satellite platforms of CrIS. It collects measurements of the land, atmosphere, cryosphere, and oceans in the 22 visible and infrared bands ranging from 0.412 to 12.01 μm [15]. It has 16 moderate-resolution bands (M-bands) with a spatial resolution of 750 m at nadir, five imaging bands (I-bands) at 375-m spatial resolution, and one panchromatic day–night band (DNB) with a 750-m spatial resolution.

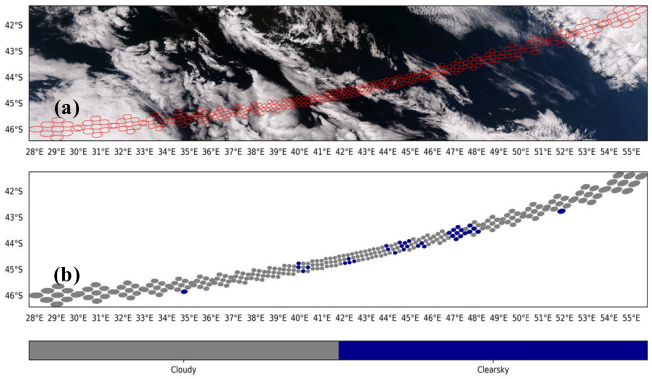

Fig. 1. Example of the collocated VIIRS and CrIS training data set selected from March 10, 2019. (a) VIIRS true-color image along with the CrIS 30 footprints (red circle) of one scan line. (b) CrIS cloud mask determined by the VIIRS cloud mask product.

The VIIRS cloud mask is determined by a series of cloud detection tests based on one or more bands [16]. The thresholds used for the cloud tests are related to region, surface type, geometry, and atmospheric condition. It has four different cloud indicators: confidently cloudy, probably cloudy, probably clear, and confidently clear. Compared to the CrIS FOV footprint size of 14 km, the VIIRS M-band cloud mask has a much higher spatial resolution of 750 m, thus providing an opportunity to check the CrIS cloud information in subpixel level. In this study, the VIIRS M-band cloud mask is used.

B. Methodology

Three major steps are conducted to build the DNN-based CrIS cloud detection model, and each one is presented.

1) Data Collocation: A fast and accurate CrIS and VIIRS collocation algorithm is integrated to obtain the training and test data sets. The VIIRS pixels within each CrIS footprint are collocated according to their line-of-sight (LOS) pointing vectors calculated with the latitude, longitude, satellite range, and satellite zenith and azimuth angles at CrIS different scan positions. An example [see Fig. 1(a)] shows one scan line of CrIS FOV footprints (red circle) overlapped with the VIIRS true-color image derived from bands M3 (0.488 μm), M4 (0.555 μm), and M5 (0.672 μm). The collocated VIIRS pixels are then used to determine the CrIS cloudy FOVs. The details of the collocation method are summarized in [17]. For general purpose, the training data set is generated from the full orbit of SNPP CrIS and VIIRS collocation data randomly selected from each month of 2018 (January 12, February 7, March 20, April 3, May 9, June 27, July 12, August 16, September 5, October 22, November 15, and December 10) with a scan and FOR interval of 3 to represent different atmospheric and surface conditions. Previous studies show that both CrIS and VIIRS are well geolocation calibrated instruments [15], [18], [19]. Their collocation accuracy is within the subpixel level less than 20 m [17]. Therefore, the geolocation error should have little impact on the cloud detection result.

2) Cloudy Scene Determination: A unitless clear-sky ratio is defined to check the CrIS FOVs and is calculated as the ratio of the number of VIIRS clear-sky pixels divided by the total number of VIIRS pixels falling in the corresponding CrIS FOVs. In this study, only confidently clear VIIRS pixels are

recognized as clear sky, whereas the others are considered as cloudy scenes. If each of the VIIRS observation is considered as a pure unit, the ratio calculated with all the VIIRS pixels within a CrIS FOV provides subpixel information to check the CrIS scene characteristics. The threshold of greater than 5%, which has been proved to be an efficient value in identifying partially cloudy scenes [9], is used to label CrIS cloudy FOVs, recognizing that the threshold in determining whether a CrIS FOV is cloudy or not, in general, is application dependent. A smaller value can be adopted if a stricter scene check is required and vice versa. For example, Wang *et al.* [20] used an even stricter threshold with all VIIRS pixels within CrIS flagged as confidently clear, to select CrIS clear-sky FOVs. In the example of the VIIRS determined CrIS cloudy scenarios [see Fig. 1(b)], most of the CrIS cloudy FOVs could be effectively identified with the proposed threshold, even the partially cloudy FOVs, through the comparison with Fig. 1(a).

3) DNN Model Building: An optimized five-layer neural network, which includes an input layer, three hidden layers, and one output layer, trains the CrIS spectra for cloud detection. The CrIS spectra are used as the predictors, while the VIIRS determined CrIS cloud mask from (2) is used as the truth for the model training as well as the following accuracy evaluation. In particular, since the channels of infrared sounder are highly correlated, the original CrIS spectra are first transformed into their principal components (PCs) and then only the first leading k PCs used as model inputs (predictors) instead of the whole 2211 channel radiances for the purpose of better regression, convergence, and faster prediction. Sensitivity test for the selection of PC numbers is conducted in Section II-C. Three fully connected hidden layers make up the central part of the DNN model, which yields the best accuracy with 512, 1024, and 64 neurons for each layer in series. Each one is trained using a rectified linear unit (RELU) function. The output layer is activated with a softmax function to map the intermediate results from the previously hidden layers to a probability distribution from 0 to 1. The CrIS FOVs with clear-sky probability value greater than 0.5 are recognized as clear sky, whereas the others are determined to be cloudy.

The DNN model is trained to optimize a categorical cross-entropy loss function via the batch gradient descent (BGD, all the training data are used to take a single iteration step) method using adaptive moment estimation [21] for 20 epochs. There are 3 663 777 training data samples, a third selected as the test data. After the DNN model is constructed, the CrIS spectra only are used to detect its cloudy scene, avoiding huge data and time consumption of the collocation preprocessing. Equation (1) shows how clouds are identified by the DNN method

$$\begin{aligned}\mathrm{CrIS}_{\mathrm{cloudmask}} &= \mathrm{Softmax}(\mathrm{Relu}(\mathrm{Relu}(\mathrm{Relu}(x_{\mathrm{pcs}} \times P_1 + W_1) \times P_2 + W_2) \\ &\quad \times P_3 + W_3)) \times P_4 + W_4)). \end{aligned} \tag{1}$$

In (1), a CrIS spectrum x is first converted into its PCs x_{pcs}. Details of the CrIS spectra PC transformation are summarized in [22]. The first leading k CrIS x_{pcs} are then multiplied with the model coefficients, to convert it into the cloud mask. $P_1, P_2, P_3,$ and P_4 and $w_1, w_2, w_3,$ and w_4 in (1) represent the weights and biases of the three fully connected hidden layers and the output layer, respectively. These coefficients are determined during the training process, by changing the numbers of hidden layers and neurons, for the best cloud detection. The RELU function bends the linear transformation to nonlinear, whereas the softmax function maps the logits from hidden layers to a probability distribution. The flowchart of the DNN-based infrared sounder cloud detection model is shown in Fig. 2.

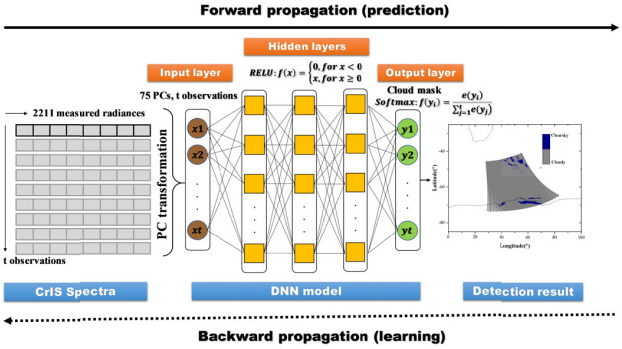

Fig. 2. Flowchart of the CrIS DNN cloud detection model.

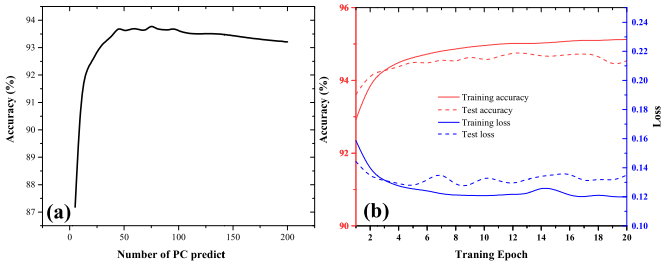

Fig. 3. (a) Sensitivity test of training accuracy versus used CrIS PCs. (b) Accuracy and loss per epoch on the training and test data sets.

C. Sensitivity Test and Accuracy Analysis

Since the channel radiances measured by infrared sounders are highly correlated, it is unnecessary to use all of them as model inputs. Principal component analysis (PCA) is an orthogonal transformation tool, which converts the correlated variables into a set of linearly uncorrelated PCs that describe the variances of the original data set. In addition, it transforms the majority of the effective signals (spectral variances) into a few leading PCs and leaves the noise information (mostly from the instrument self) nearly equally distributed into all the PCs. By only using the leading k PCs as predictors instead of all the dependent explanatory variables, the dimension and instrument noise of the measurements is greatly reduced, achieving the goal of model optimization (e.g., data deduction, training optimization, and computing acceleration). In this study, a sensitivity test determines the number of PCs used for the models. As shown in Fig. 3(a), the training model accuracy (calculated in one BGD iteration step) shows an increasing trend with the increase of used PCs. The model accuracy is defined as the probability of the correct prediction of both cloudy and clear-sky scenes by the model. However, a slightly decreasing trend was observed after around 75 PCs of the "knee point." This is attributed to the instrument noise (which begins to dominate the PC signals), and the training result would not be improved by adding more PCs to the model. Therefore, the top 75 PCs of the CrIS spectra are finally selected as the predictors for the DNN cloud detection.

The model performance is further discussed by using the selected 75 PC predictors. Fig. 3(b) shows the model accuracy

and loss as a variable of the training epoch on the training and test data separately. A loss generally conveys how well it behaves after each iteration of optimization. As clearly shown, the model accuracy (red lines with the Y-axis in the left) slightly increased from 93% to 95% along with the increase of training iteration steps. The accuracy curve calculated from test data is only slightly lower than that of the training data set globally (less than 0.5%), implying that the model has been well generalized without obvious underfitting. Moreover, to diagnose whether the model is overfitted, their loss curves are also investigated as the blue lines illustrate (Y-axis in the right). The training and test loss are very similar in the first five training epochs. After that, the test loss shows a small increasing trend with more training epochs performed. The gap between training and test curves indicate that the model learned the training data set too well after five training epochs and is overfitted. Accordingly, the training process was terminated at the smallest test loss to avoid potential overfitting.

In addition, sensitivity test is performed on the training data set to see whether it could have a general representative of the global scenes. Three independent training data sets of four-day randomly selected from different seasons, six-day randomly selected every two months, and 12-day randomly selected from each month are used to train the DNN model separately. The DNN models trained by different training samples are then tested with the same test data set. Similar cloud detection results are achieved from the trained DNN models. As a result, the increase of training data samples (from four days of different seasons to 12 days of a whole year) does not bring obvious improvement in the cloud detection result, which implies that the training samples used in study are sufficient.

III. Case Study and Analysis

One day of CrIS and VIIRS collocation data (March 10, 2019), which was not included in the training data set, is investigated to further test the performance of the CrIS DNN cloud detection model. The truth of the CrIS cloud mask is determined by the collocated VIIRS cloud product with the methodology discussed in Section II. The results are plotted in Fig. 4.

As the VIIRS true-color imagery [see Fig. 4(a)] shown, massive clouds are observed over the land and ocean surfaces globally. From the CrIS cloud mask determined by the VIIRS cloud product [see Fig. 4(b)] and through the comparison with the true-color imagery, most of the CrIS cloudy scenarios are correctly detected by the VIIRS cloud product. The purely clear-sky FOVs of CrIS are mainly located in southern Argentina, Sahara Desert of Africa, and Australia from west to east. Given the CrIS cloud detection result from the proposed DNN model [see Fig. 4(c)] compared that in Fig. 4(b), the majority of CrIS cloudy FOVs are also successfully identified by the DNN model. The overall accuracy for this one-day testing data is 93% (which is similar to the model accuracy discussed at the training stage), with a relatively higher (94%) and lower (91%) accuracy in the daytime and nighttime (not shown), respectively. It is reasonable to see a higher accuracy in the daytime data because the received signals of CrIS are stronger in the daytime than in nighttime, which makes the spectral contrast between clear-sky and cloudy areas much stronger in the daytime. The model's false detections are further shown in Fig. 4(d). The false positive

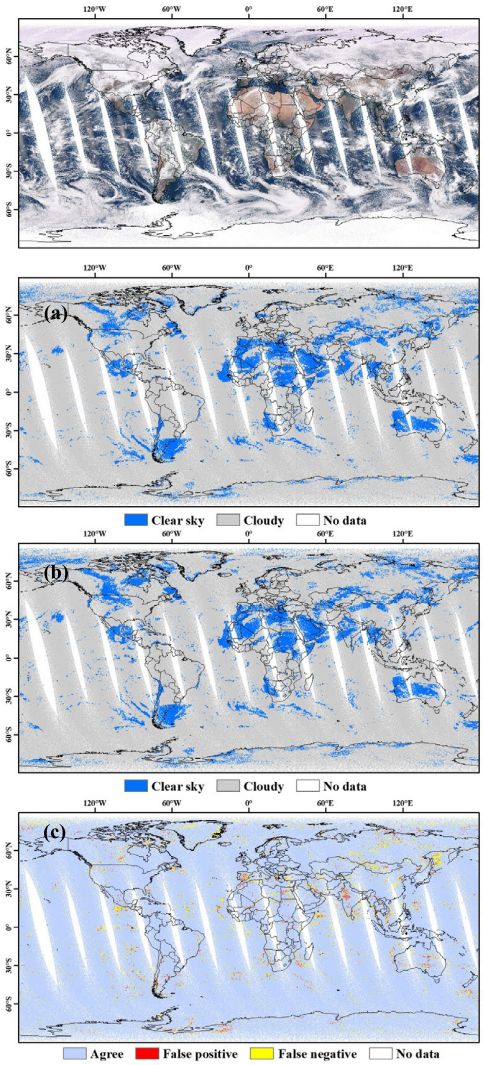

Fig. 4. (a) VIIRS true-color imagery measured on the daytime of March 10, 2019. (b) CrIS cloud detection result determined by VIIRS cloud mask (Truth). (c) CrIS cloud detection result identified by the proposed DNN method. (d) Difference between (b) and (c).

represents that a truth clear-sky FOV is predicted as cloudy; on the contrary, the false negative means that a truth cloudy scene is recognized as clear sky by the model. In general, the model has a better accuracy over ocean (95%) than that of the land (88%). This is due to the surface cover over upland landscapes which is more complicated than that of oceans. The land mixed-pixel issue increases the difficulty of cloud detection. Especially, it is found that sometimes the DNN model would recognize certain thin cloud as clear sky because the spectrum of thin cloud is very similar to that of the clear sky. Moreover, the false detected pixels are also found over snow- or ice-covered and desert areas. This is possibly due to the VIIRS cloud mask (which is used as the truth) that has a relatively low accuracy over these areas (~86% in desert, ~88% in snow-covered land, and 72% in Antarctic and Greenland [23]). The false inputs from VIIRS over these scenarios will give the wrong information to the model during the training process, thus reducing model's ability in correctly detecting clouds over these areas. In addition, it is also worthy to note that the cutoff of PCs may have some negative impacts on the model accuracy, as some of the useful information may

potentially be lost along with the abandoned PCs. However, considering the advantages of PCA and the data characteristics of hyperspectral infrared sounder, it is still worthy to do the PC transformation to optimize the model inputs, and the sensitivity test in Section II suggests that it is unnecessary to use more PC predictors in the model. Further case validations are also performed over different months (not shown), and the results show that the model accuracy has a small variation ranging from 92% to 94%, with an average of 93%. These tests demonstrate that the DNN model is stable and could be an effective tool for the CrIS cloud detection.

IV. Conclusion

A new cloud detection model is built for the hyperspectral infrared sounder of CrIS. Different from previous cloud detection methods such as the radiative transfer model-based clear-sky selection methods [3], [4], we combined microwave and infrared sounder cloud clearing methods [5], [6], as well as the subpixel cloud detection methods [7]–[9], and developed the approach based on the state-of-the-art artificial DNN. The proposed DNN model uses the cloud information measured from the imager to train the sounder spectra, which greatly enhances the efficiency of the cloud detection algorithm, even though there is a slight tradeoff in accuracy. It allows us to reach the CrIS cloud detection accuracy of 93% globally through the comparison with the VIIRS. The high consistency between results from the proposed model and the truth indicates that the new model could effectively identify the cloudy scene from hyperspectral infrared sounders. Finally, the methodology is easily adapted by other hyperspectral infrared sensors, such as training AIRS using MODIS measurements and IASI using AVHRR observations. In addition, the proposed DNN cloud detection method can be applied to other nonhyperspectral satellite instrument pairs if a lower spatial resolution sensor could be spatiotemporally collocated with a higher spatial resolution instrument in a similar manner. Further investigation of this approach could foster the adoption of the methodology in an operational mode for big spatiotemporal remote sensing data analytics [24].

Acknowledgment

The authors gratefully acknowledge the anonymous reviewers who have offered constructive feedback. The scientific satellite data are obtained from the NOAA Comprehensive Large Array Data Stewardship System.

References

[1] Y. Han and Y. Chen, "Calibration algorithm for cross-track infrared sounder full spectral resolution measurements," *IEEE Trans. Geosci. Remote Sens.*, vol. 56, no. 2, pp. 1008–1016, Feb. 2018, doi: 10.1109/TGRS.2017.2757940.

[2] P. Bauer *et al.*, "Satellite cloud and precipitation assimilation at operational NWP centres," *Quart. J. Roy. Meteorological Soc.*, vol. 137, no. 661, pp. 1934–1951, Oct. 2011, doi: 10.1002/qj.905.

[3] A. P. McNally and P. D. Watts, "A cloud detection algorithm for high-spectral-resolution infrared sounders," *Quart. J. Roy. Meteorol. Soc.*, vol. 129, pp. 3411–3423, Apr. 2003, doi: 10.1256/q.j.02.208.

[4] L. Lin, X. Zou, and F. Weng, "Combining CrIS double CO_2 bands for detecting clouds located in different layers of the atmosphere," *J. Geophys. Res. Atmos.*, vol. 122, no. 3, pp. 1811–1827, Feb. 2017, doi: 0.1002/2016JD025505.

[5] J. Susskind, C. D. Barnet, and J. M. Blaisdell, "Retrieval of atmospheric and surface parameters from AIRS/AMSU/HSB data in the presence of clouds," *IEEE Trans. Geosci. Remote Sens.*, vol. 41, no. 2, pp. 390–409, Feb. 2003.

[6] G. Antonia. (Aug. 2017). *The NOAA Unique Combined Atmospheric Processing System (NUCAPS) Algorithm Theoretical Basis Document, Version 2.0*. [Online]. Available: https://www.star.nesdis.noaa.gov/jpss/documents/ATBD/ATBD_NUCAPS_v2.0.pdf

[7] J. Li, W. P. Menzel, F. Sun, T. J. Schmit, and J. Gurka, "AIRS subpixel cloud characterization using MODIS cloud products," *J. Appl. Meteorol.*, vol. 43, pp. 1083–1094, Apr. 2004, doi: 10.1175/1520-0450(2004)043<1083:ASCCUM>2.0.CO.2.

[8] R. Eresmaa, "Imager-assisted cloud detection for assimilation of infrared atmospheric sounding interferometer radiances: Imager-assisted cloud detection for radiance assimilation," *Quart. J. Roy. Meteorological Soc.*, vol. 140, no. 684, pp. 2342–2352, Oct. 2014, doi: 10.1002/qj.2304.

[9] P. Wang, J. Li, Z. Li, A. H. N. Lim, J. Li, and T. J. Schmit, "The impact of cross-track infrared sounder (CrIS) cloud-cleared radiances on hurricane Joaquin (2015) and Matthew (2016) forecasts," *J. Geophys. Res., Atmos.*, vol. 122, pp. 13201–13218, Dec. 2017, doi: 10.1002/2017JD027515.

[10] C. Yang *et al.*, "Big Earth data analytics: A survey," *Big Earth Data*, vol. 3, no. 2, pp. 83–107, May 2019, doi: 10.1080/20964471.2019.1611175.

[11] M. Yu *et al.*, "Spatiotemporal event detection: A review," *Int. J. Digit. Earth*, Mar. 2020, doi: 10.1080/17538947.2020.1738569.

[12] M. Xu *et al.*, "PreciPatch: A dictionary-based precipitation downscaling method," *Remote Sens.*, vol. 12, no. 6, p. 1030, Mar. 2020, doi: 10.3390/rs12061030.

[13] S. Li, W. Song, L. Fang, Y. Chen, P. Ghamisi, and J. A. Benediktsson, "Deep learning for hyperspectral image classification: An overview," *IEEE Trans. Geosci. Remote Sens.*, vol. 57, no. 9, pp. 6690–6709, Sep. 2019, doi: 10.1109/TGRS.2019.2907932.

[14] Q. Liu *et al.*, "Daytime rainy cloud detection and convective precipitation delineation based on a deep neural network method using GOES-16 ABI images," *Remote Sens.*, vol. 11, no. 21, p. 2555, Oct. 2019, doi: 10.3390/rs11212555.

[15] C. Cao *et al.*, "Suomi NPP VIIRS sensor data record verification, validation, and long-term performance monitoring," *J. Geophys. Res. Atmos.*, vol. 118, no. 22, pp. 11664–11678, Nov. 2013, doi: 10.1002/2013JD020418.

[16] T. J. Kopp *et al.*, "The VIIRS cloud mask: Progress in the first year of S-NPP toward a common cloud detection scheme," *J. Geophys. Res., Atmos.*, vol. 119, no. 5, pp. 2441–2456, Mar. 2014, doi: 10.1002/2013JD020458.

[17] L. Wang, D. Tremblay, B. Zhang, and Y. Han, "Fast and accurate collocation of the visible infrared imaging radiometer suite measurements with cross-track infrared sounder," *Remote Sens.*, vol. 8, no. 1, p. 76, Jan. 2016, doi: 10.3390/rs8010076.

[18] L. Wang *et al.*, "Geolocation assessment for CrIS sensor data records," *J. Geophys. Res. Atmos.*, vol. 118, no. 22, pp. 12690–12704, 2013, doi: 10.1002/2013JD020376.

[19] L. Wang, B. Zhang, D. Tremblay, and Y. Han, "Improved scheme for cross-track infrared sounder geolocation assessment and optimization," *J. Geophys. Res., Atmos.*, vol. 122, no. 1, pp. 519–536, Jan. 2017, doi: 10.1002/2016JD025812.

[20] L. Wang, Y. Chen, and Y. Han, "Impacts of field of view configuration of cross-track infrared sounder on clear-sky observations," *Appl. Opt*, vol. 55, no. 25, pp. 7113–7119, Sep. 2016, doi: 10.1364/AO.55.007113.

[21] D. P. Kingma and J. Ba, "Adam: A method for stochastic optimization," in *Proc. Int. Conf. Learn. Represent.*, San Diego, CA, USA, May 2015, pp. 1–13.

[22] H. Xu, Y. Chen, and L. Wang, "Cross-track infrared sounder spectral gap filling toward improving intercalibration uncertainties," *IEEE Trans. Geosci. Remote Sens.*, vol. 57, no. 1, pp. 509–519, Jan. 2019, doi: 10.1109/TGRS.2018.2857833.

[23] L. Zhou, M. Divakarla, X. Liu, A. Layns, and M. Goldberg, "An overview of the science performances and calibration/validation of Joint Polar Satellite System operational products," *Remote Sens.*, vol. 11, no. 6, p. 698, Mar. 2019, doi: 10.3390/rs11060698.

[24] C. Yang *et al.*, "Big spatiotemporal data analytics: A research and innovation frontier," *Int. J. Geogr. Inf. Sci.*, vol. 34, pp. 1075–1088, Dec. 2019, doi: 10.1080/13658816.2019.1698.